BLADE-ELEMENT PERFORMANCE OF 0.7 HUB-TIP RADIUS RATIO AXIAL-FLOW-PUMP ROTOR WITH TIP DIFFUSION FACTOR OF 0.43

by James E. Crouse and Donald M. Sandercock

Lewis Research Center
Cleveland, Ohio

BLADE-ELEMENT PERFORMANCE OF 0.7 HUB-TIP RADIUS

RATIO AXIAL-FLOW-PUMP ROTOR WITH TIP

DIFFUSION FACTOR OF 0.43

By James E. Crouse and Donald M. Sandercock

Lewis Research Center
Cleveland, Ohio

NATIONAL AERONAUTICS AND SPACE ADMINISTRATION

BLADE-ELEMENT PERFORMANCE OF 0.7 HUB-TIP RADIUS

RATIO AXIAL-FLOW-PUMP ROTOR WITH TIP

DIFFUSION FACTOR OF 0.43

by James E. Crouse and Donald M. Sandercock

Lewis Research Center

SUMMARY

A 9-inch-diameter axial-flow pump was tested in water. The double-circular-arc-bladed rotor had a hub-tip radius ratio of 0.7, tip solidity of 1.02, and design D-factors of 0.43 and 0.70 at the tip and hub, respectively. The investigation covered operations under both noncavitating and cavitating conditions. Radial surveys of flow conditions at the rotor inlet and outlet were taken, and performance across a selected number of blade elements was computed and presented.

The largest variation of blade-element performance parameters with inlet flow occurred in the blade tip region, thus indicating the criticality of design in this area. Over the upper 30 percent of blade height, loss-coefficient distributions with incidence angles for this rotor configuration indicated that positive blade stall (sharp increase in loss coefficient) occurred very close to the minimum-loss incidence angle, but the loss coefficient increased very slowly moving from reference incidence angle toward a negative stall condition.

At design flow the design and measured performance compared favorably at all radial locations except at the tip element. Because of a decrease in the inlet-flow coefficient at this element (probably due to casing boundary layer), the tip rotor element operated at an incidence angle above the design value and very close to a blade stall condition. Consequently, the tip-region performance showed significant deviations from the predicted design values. Furthermore, although at design flow most of the blade elements were operating near their respective minimum-loss operating points, the flow margin between design and blade stall was small.

The measured pump rotor performance is compared with predicted values using the design procedures of reference 1. The sensitivity of the design procedure at high inlet-flow angles is demonstrated, and the need for additional data and/or modifications to the design system for use in the high inlet-flow angle area is indicated.

Tests under cavitating conditions showed that the effects of cavitation on rotor blade performance were first noted at a cavitation number of approximately 0.19.

INTRODUCTION

The success of the design of an axial-flow-pump rotor (or stator) depends primarily on the ability to predict accurately the following:

(1) Deviation of the fluid-flow angles from the blade angles

(2) Level of loss of the flow process through the cascades of blades

(3) Incidence angle (or angle of attack) at which the loss is in a minimum-loss range

Considerations of maximum blade loading, flow range, and stability generally guide the selection of the previous basic parameter values. Finally, the blade elements should be matched for overall optimum design.

In reference 1 the blade-element performance from a large number of cascades and rotors utilizing air as the test fluid are correlated, and empirical rules for predicting minimum-loss incidence angle, deviation angle, and loss are formulated. The overall and blade-element performance of an axial-flow rotor pumping water is presented in references 2 and 3. In addition to the differences of fluids and flow velocities, the most significant difference from the data of reference 1 is the large blade stagger angles (or inlet angles) at which the water pump operates as compared to those used by air-compressor rotor blades. Comparisons of the observed results of this pump rotor operating in water with those predicted from the design rules presented in reference 1 are made.

To evaluate further the utility of applying the data of reference 1 to the design of axial-flow pumps, the performance of this second pump rotor was investigated. This rotor had a higher level of blade loading and a higher hub-tip radius ratio than that reported in reference 2. The design and overall performance of this rotor are reported in reference 4. This report presents the performance of the individual blade elements and compares it with the design criteria of reference 1. Cavitation performance is also presented.

APPARATUS AND PROCEDURE

The rotor design procedure, test facility, instrumentation, and test methods are presented in some detail in reference 2; consequently, only a brief resume of salient points will be made herein. (All symbols are defined in appendix A.)

Rotor Design

The pump rotor was 9 inches in diameter with a 0.7 hub-tip radius ratio.

TABLE I. - RADIAL DISTRIBUTIONS OF DESIGN PARAMETERS

[Rotor tip diameter, 9.00 inches; number of
blades, 19.]

Rotor hub-tip radius ratio r/r_t	Diffu-sion factor, D	Inci-dence angle, i, deg	Devia-tion angle, δ, deg	Camber angle, φ, deg	Solidity, σ	Chord, C, in.	Setting angle, γ	Ratio of maximum thickness to chord, t_{max}/C
Tip 1.00	0.426	6.4	4.6	0	1.01	1.52	67.1	0.0700
.95	.433	2.0	5.4	11.8	1.06		64.9	.0725
.90	.464	.9	6.9	16.4	1.12		62.8	.0750
.85	.505	.5	7.8	19.8	1.19		60.5	.0775
.80	.555	.6	8.3	22.1	1.26		58.2	.0800
.75	.615	1.0	8.8	24.6	1.35		55.3	.0825
Hub .70	.693	1.2	9.3	27.6	1.44		52.2	.0850

The design utilized a blade element concept with design calculations made across a selected number of blade elements. These are then stacked to form a blade.

The velocity diagrams were constructed utilizing the following assumptions and selections:

(1) No inlet whirl ($V_{\theta,1} = 0$)

(2) Inlet relative flow angle of 73.6° at the tip (ideal inlet-flow coefficient of 0.294 when combined with (1))

(3) Inlet-flow coefficient φ_1 constant at all radii

(4) Radially constant energy addition ($\psi_i = 0.294$)

(5) Assumed radial distribution of loss coefficient

(6) Radial equilibrium ($\partial h/\partial r = V_{\theta}^2/gr$)

Double-circular arc-blade shapes (circular-arc camber line) were selected to establish the de-
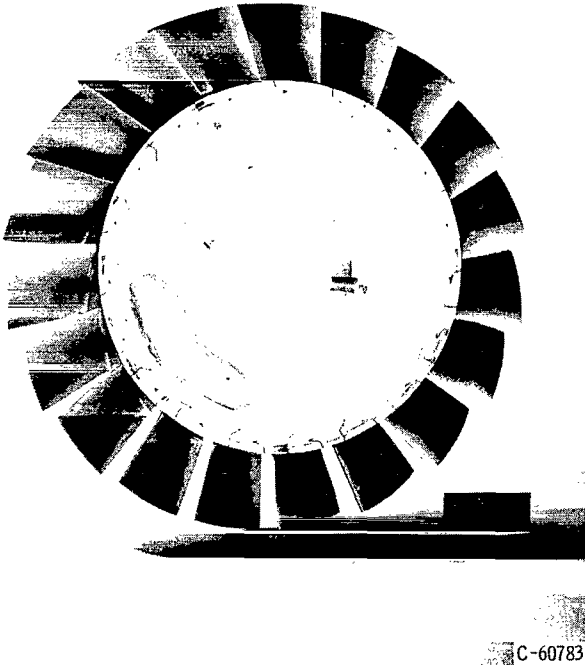

C-60783

Figure 1. - Rotor.

3

sired flow conditions. Blade incidence and deviation angle were computed from the equations of reference 1 with slight modifications as described in reference 4.

Radial distributions of significant design parameters are given in table I and on the performance figures. A photograph of the rotor is shown in figure 1.

Test Facility

The pump performance was investigated in the Lewis Research Center water tunnel. The major components of this facility are shown schematically in figure 2. During operation the gas content remains below 3 parts per million by weight. The filtering system is capable of removing solid matter larger than 5 microns.

Test Procedure and Instrumentation

The test procedure consisted of setting flow, speed, and inlet pressure and then obtaining radial surveys of total and static heads plus flow angle at the blade inlet and outlet. The survey instruments shown in figure 3 consisted of a claw-type probe that measured total pressure and angle and a wedge-type probe that measured static pressure and angle. Measuring stations were located approximately 1 inch upstream and downstream of the blade leading and trailing edge, respectively. A head calibration factor for each static wedge
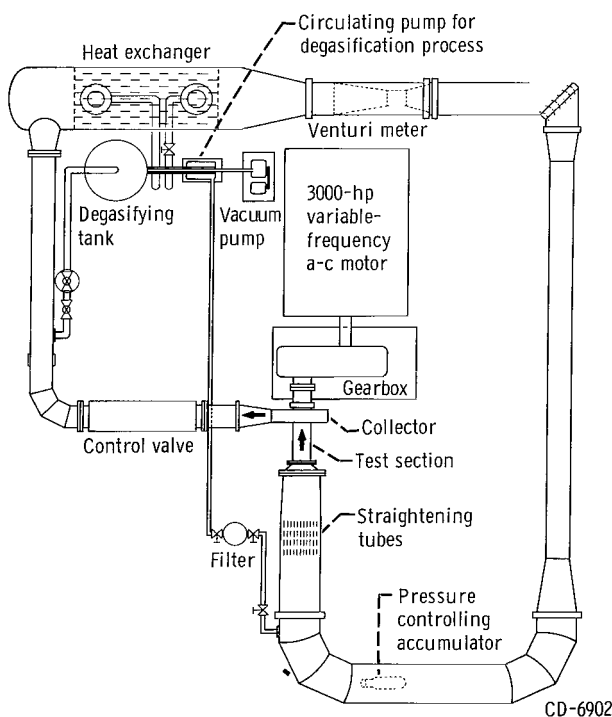
Figure 2. - Lewis water tunnel.

(a) Total-pressure claw.
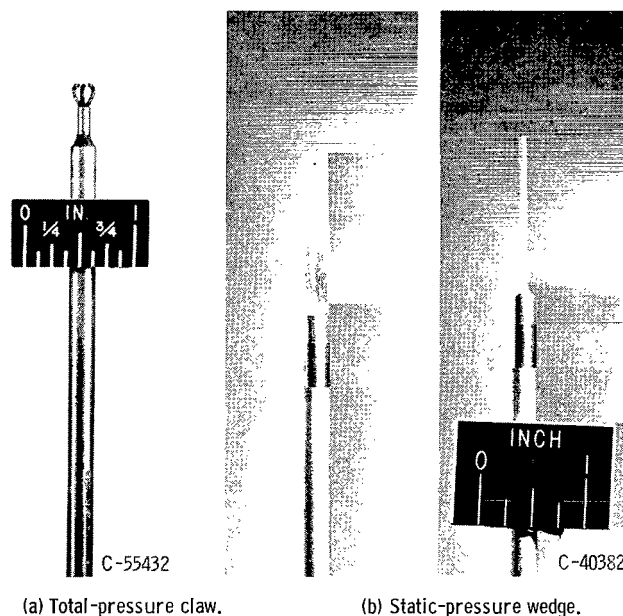C-55432

(b) Static-pressure wedge.
C-40382

Figure 3. - Probes.

was determined in an air tunnel and applied to the measured static pressures in the water tunnel. Rotor speed was obtained from an electronic speed counter used in conjunction with a magnetic pickup, and flow was measured by means of a venturi flowmeter. Water temperature was maintained at a constant value of approximately 80° F. The estimated accuracy of the following measurements represents the inherent accuracy of the measuring and recording devices employed:

Flow rate, Q, percent . . . . < ±1.0
Rotative speed, N, percent . . . . ±0.5
Head rise, ΔH, percent of full scale . . . . < ±0.5
Flow angles, β, deg . . . . ±1.0

Discrepancies arising from unsteady flow conditions, circumferential variations of flow, cavitation on the probes, etc., could not be evaluated.

The equations necessary for calculation of the desired performance parameters are presented in appendix B.

Figure 4 provides some check on the reliability of the data by comparing

(a) Inlet measuring station.   (b) Outlet measuring station.
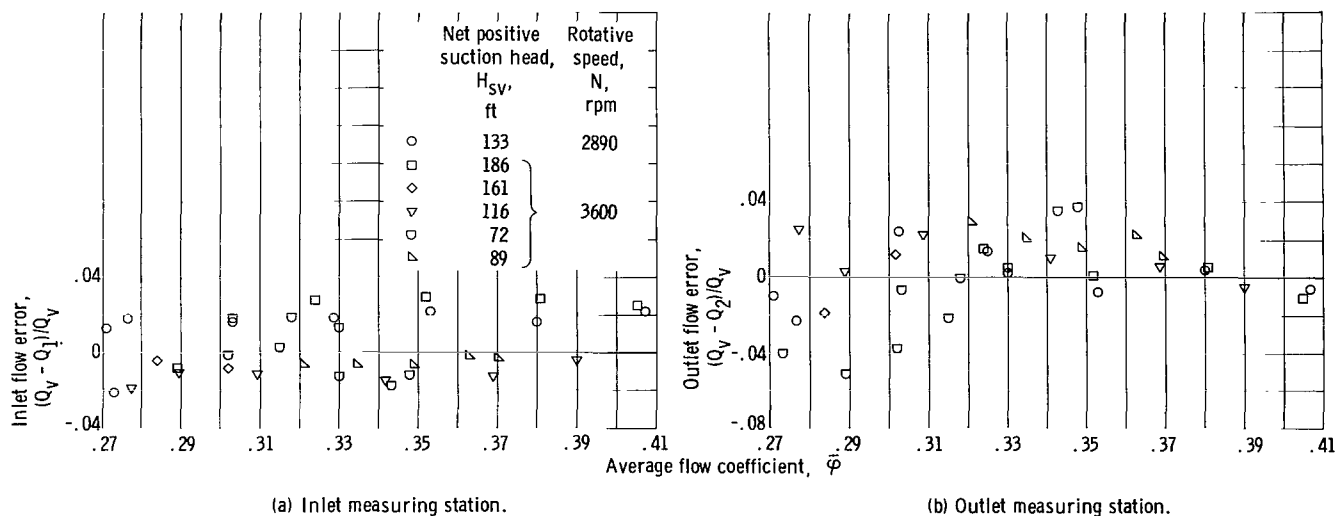
Figure 4. - Comparison of integrated weight flows at blade inlet and outlet with those measured by venturi meter.

the integrated weight flows at the blade inlet and outlet with those measured by the venturi flowmeter. The comparisons at both the inlet and outlet measuring stations are considered good and presage confidence in the validity of the observed flow measurements.

Selection of Blade-Element Parameters for Analysis

The analysis of rotor performance parallels the design procedure in that individual element performance is analyzed and then integrated to obtain the overall blade row performance. Through a given blade passage the flow patterns are primarily affected by

(1) Incidence angle

(2) Deviation angle

(3) Loss level, or loss coefficient

As a measure of the blade loading, the diffusion factor D defined and developed in reference 5 is utilized. The cavitation number k provides a measure of the susceptibility of the blades to cavitation. The amount of turning of the fluid done by a given blade row is computed from the relation

$$\Delta\beta' = i + \varphi^O - \delta$$

The energy addition imparted to the fluid by the rotor blades is shown as an ideal head-rise coefficient ψ_i and is dependent on the fluid turning and axial velocity changes (see eqs. (B1) and (B7) of appendix B). Accordingly, to support both design and analysis procedures and to permit reproduction of desired velocity diagrams, the data are presented in terms of the following blade-element parameters:

(1) Head-rise coefficient ψ

(2) Ideal head-rise coefficient ψ_i

(3) Efficiency η

(4) Incidence angle i

(5) Deviation angle δ

(6) Loss coefficient $\bar{\omega}$

(7) Diffusion factor D

(8) Flow coefficient φ

(9) Cavitation number k

(10) Fluid-flow angle β

All parameters are defined by the equations of appendix B.

RESULTS AND DISCUSSION

An initial step in an investigation of this type is the determination of an inlet pressure (compatible with rotor speed) above which the measured performance is not affected by cavitation, or vapor formation, occurring in the flow passages around the blade. Operation above and below this pressure is defined herein as noncavitating and cavitating, respectively. Performance observed under these two types of operation will be presented and discussed in

separate sections.

For this particular rotor operating in water at a blade tip speed of 141.5 feet per second, as the system head was reduced the initial effects of cavitation on measured rotor performance occurred at an inlet head of approximately 117 feet (corresponding to a suction specific speed of approximately 7600). At these operating conditions cavitation on the blade surface and in the tip vortex was visible through a transparent acrylic plastic casing. Increasing the inlet pressure to 160 feet eliminated the blade surface cavitation but not all the tip vortex cavitation; hence, performance obtained at an inlet head of 160 feet (or greater) is presented herein as noncavitating.

In general, the curves presented are self-explanatory and only points of special significance will be discussed.

Noncavitating Performance

Overall performance. - The noncavitating overall performance is presented in figure 5 with mass-averaged head-rise coefficient $\bar{\psi}$ and efficiency $\bar{\eta}$
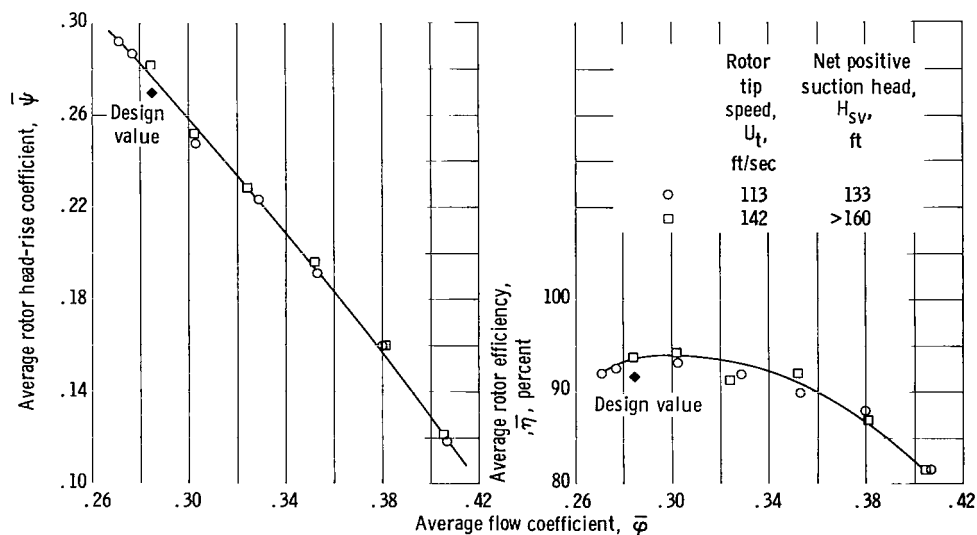
Figure 5. - Overall performance of axial-flow-pump rotor for noncavitating conditions.

shown as functions of flow coefficient $\bar{\varphi}$. Design values are included for comparison. Since the overall performance is discussed in reference 4, only the major points are repeated briefly herein.

At design-flow coefficient (assuming a 3-percent boundary layer blockage factor) the rotor produced a slightly higher-than-design head rise at a higher-than-design efficiency. If the whole range of operations is considered, three significant performance features are noted for this rotor, namely,

(1) High level of efficiency

(2) Relatively wide range of operation over which a high efficiency
(>0.90) was attained

(3) Small flow margin between the design point and an operating condition
($\bar{\varphi}$ = 0.271) below which excessive rig vibrations prevented prolonged
operation

Blade-element performance. - Figure 6 presents the radial distributions
of flow and selected blade-element performance parameters for a range of oper-
ating conditions. This type of plot displays the radial distributions of flow
and radial matching of blade-element performance under various modes of oper-
ation. It also indicates the range of inlet-flow conditions a succeeding sta-
tor row would be required to accept.

Over the range of flow covered by figure 6, the inlet conditions show no
significant change in the radial distributions of flow parameters. Axial ve-
locities are nearly constant across the passage with the small dropoff in the
tip region probably due to effects of casing boundary layer. Reference 4 also
showed a decrease in inlet total head at this station for all operating condi-
tions. Prerotation of the fluid is small at all operating points and, in gen-
eral, increases slightly as flow is decreased.

The radial distribution of outlet-flow conditions and performance relates
the individual element performances through the radial equilibrium require-
ments. To construct the radial distribution of outlet-flow conditions and per-
formance at a given inlet flow, some knowledge of the variation of deviation
angle and loss with incidence angle for each element must be available. (This
type of information is presented later in this section.) The radial distribu-
tions of outlet-flow conditions and element performance for this rotor indicate
that the blade tip region displays the greatest sensitivity to changes in
inlet-flow coefficient. The following observations are made:

(1) For any given value of blade loading (as indicated by D-factor val-
ues), the level of loss measured in the tip region is several times that ob-
served at any other radial location. This indicates the occurrence of tip
clearance and secondary flows and their effects on the level of loss in this
region.

(2) The energy addition variation with inlet flow coefficient is consider-
ably larger in the tip region than at other radial stations. A simple velocity
diagram analysis, assuming the deviation angles or outlet-relative-flow angles
remain constant, indicates that for a given change of outlet-flow coefficient
the energy addition ψ_i change will be greater as the outlet-relative-flow
angle increases. In an actual application, however, the changes obtained from
these idealized calculations are tempered by radial equilibrium requirements
and the effects of the radial gradient of loss on the radial variation of axial
velocity.

(3) The effects of the radial variations of loss coefficient are observed
on both the distributions of actual head-rise coefficient ψ and outlet-flow
coefficient φ_2. In both cases the gradients in the tip region are less than
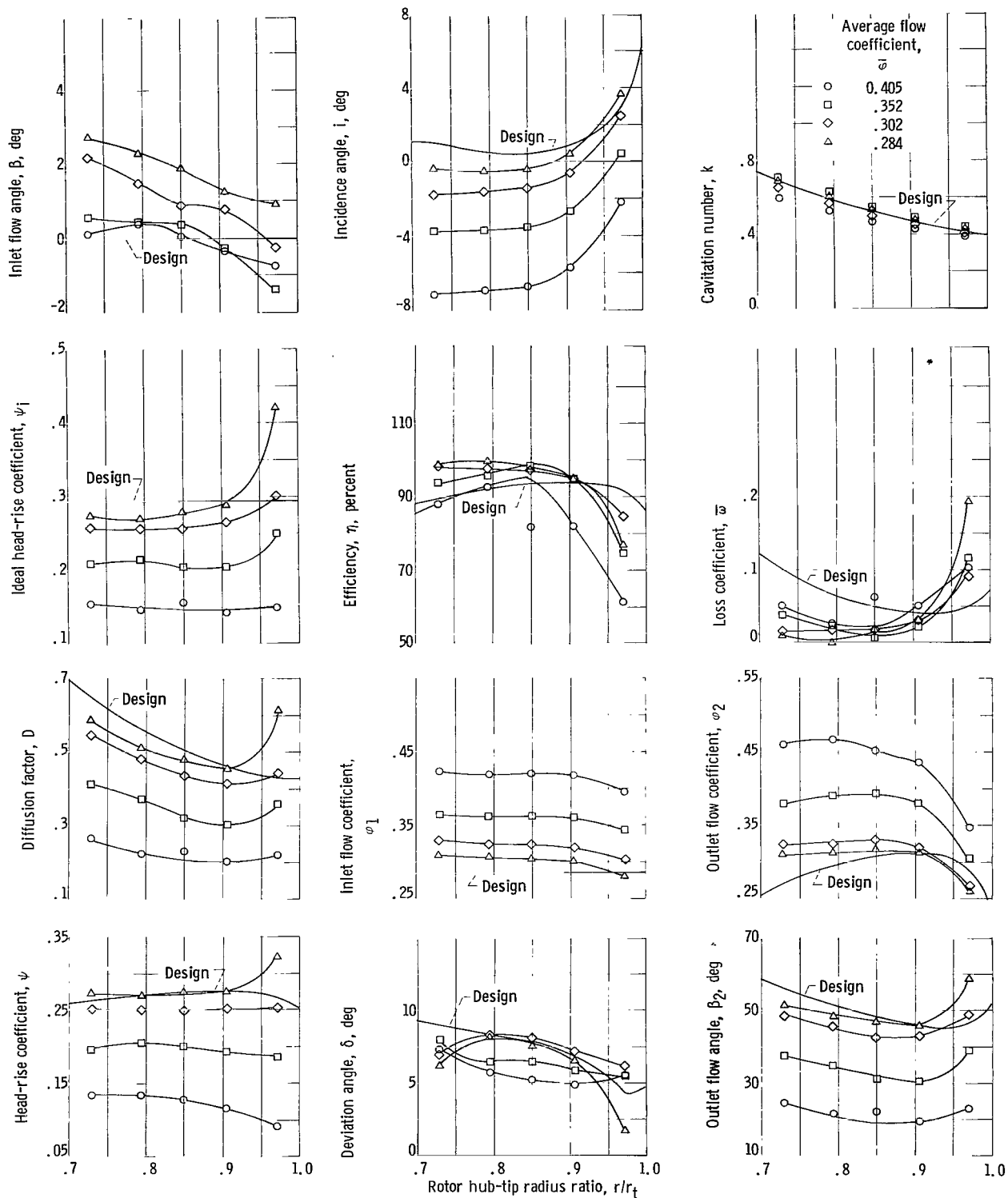
Figure 6. – Radial distributions of flow and blade-element performance parameters for noncavitating conditions. Rotor tangential velocity at tip, 141.5 feet per second; net positive suction head, >160 feet.

might be expected from the observed sharp gradients of energy addition. This is noted particularly when comparing radial distributions at inlet-flow coefficients of 0.302 and 0.284.

For comparison with design, the data obtained at a flow coefficient of 0.284 (design $\overline{\varphi} = 0.282$) are used. At the inlet the effects of casing boundary layer on the velocity in the tip regions resulted in a lower-than-design axial velocity at the tip and a slightly higher-than-design axial velocity at all other stations. This is responsible for the comparison of design and measured incidence angle shown. Small positive-flow angles ($<3^{\circ}$) were measured at all radii in comparison to the design assumption of no inlet whirl. At the design level of performance at the hub measuring station ($r/r_t = 0.728$) an inlet-flow angle of 2.7° results in a difference of 0.5° in incidence angle and a 3- to 4-percent difference in energy addition.

The outlet distributions of flow conditions and performance parameters show that the largest variations from design are occurring in the tip region. The energy addition ψ_i is significantly higher than the design value because both deviation angle δ and outlet-flow coefficient φ_2 are lower than design. Although the loss coefficient $\overline{\omega}$ is also higher than design, the resulting effect is a higher-than-design head-rise coefficient, but at a lower-than-design efficiency. The reason for the low value of deviation angle at this tip element is not readily explained. The sharp increase in loss coefficient at the design flow over other flow conditions indicates that the tip element may be in, or close to, a stalled condition. If so, a measurement error would not be unexpected, although the overall integrated and venturi measured flows check very closely at this operating condition.

At all other elements the differences between the design and the observed values of blade-element parameters are in the same direction, as noted on the curves. In general, the predicted (design) loss coefficients exceeded the observed values (especially in the hub region); although the measured energy addition was lower than design, the measured and design values of head-rise coefficient compared favorably at all radii. The relatively low values of loss coefficient for all but the tip element seem to indicate that most of the elements are reasonably well matched (operating close to minimum loss) at the design flow point.

The comparison illustrates the sensitivity of design of blade elements with high inlet angles. A variation of 1° in incidence or deviation angle results in significant changes in the ideal head-rise coefficient ψ_i for this type velocity diagram. This in turn affects both the level of element performance and radial equilibrium requirements. In addition, it also indicates the need for precise experimental techniques and instrumentation when obtaining survey data of this type.

The performance of the individual blade elements as functions of incidence angle is presented in figure 7. This type of plot is used in the analysis and design of individual blade elements.

As noted earlier, the basic parameters used in a rotor design are minimum-

10

loss incidence angles plus the loss level and deviation angle at the reference incidence angle. At radial positions 1 and 2 (r/r_t = 0.971 and 0.906, respectively) the flow ranges covered defined minimum-loss incidence angles reasonably well. Both of these blade elements display a very sharp increase in loss on the positive (high incidence) side of the minimum-loss point and a gradual increase in loss on the negative (low incidence) side of the minimum-loss point. At the remaining radial measuring stations minimum-loss incidence angles are not well defined, but all elements show a relatively small increase in loss on the negative side of minimum-loss incidence angle. As a result of this particular variation of loss from the minimum-loss point to higher incidence angles, at both radial positions 1 and 2 the maximum efficiency and minimum loss occur at the same incidence angle.

Certain basic performance trends on blades tested in a two-dimensional cascade are reported in reference 6. Inlet flow angles up to 70° are covered. From these cascade tests the recommended design angle of attack is selected by examining measured blade surface pressure gradients and designating the angle
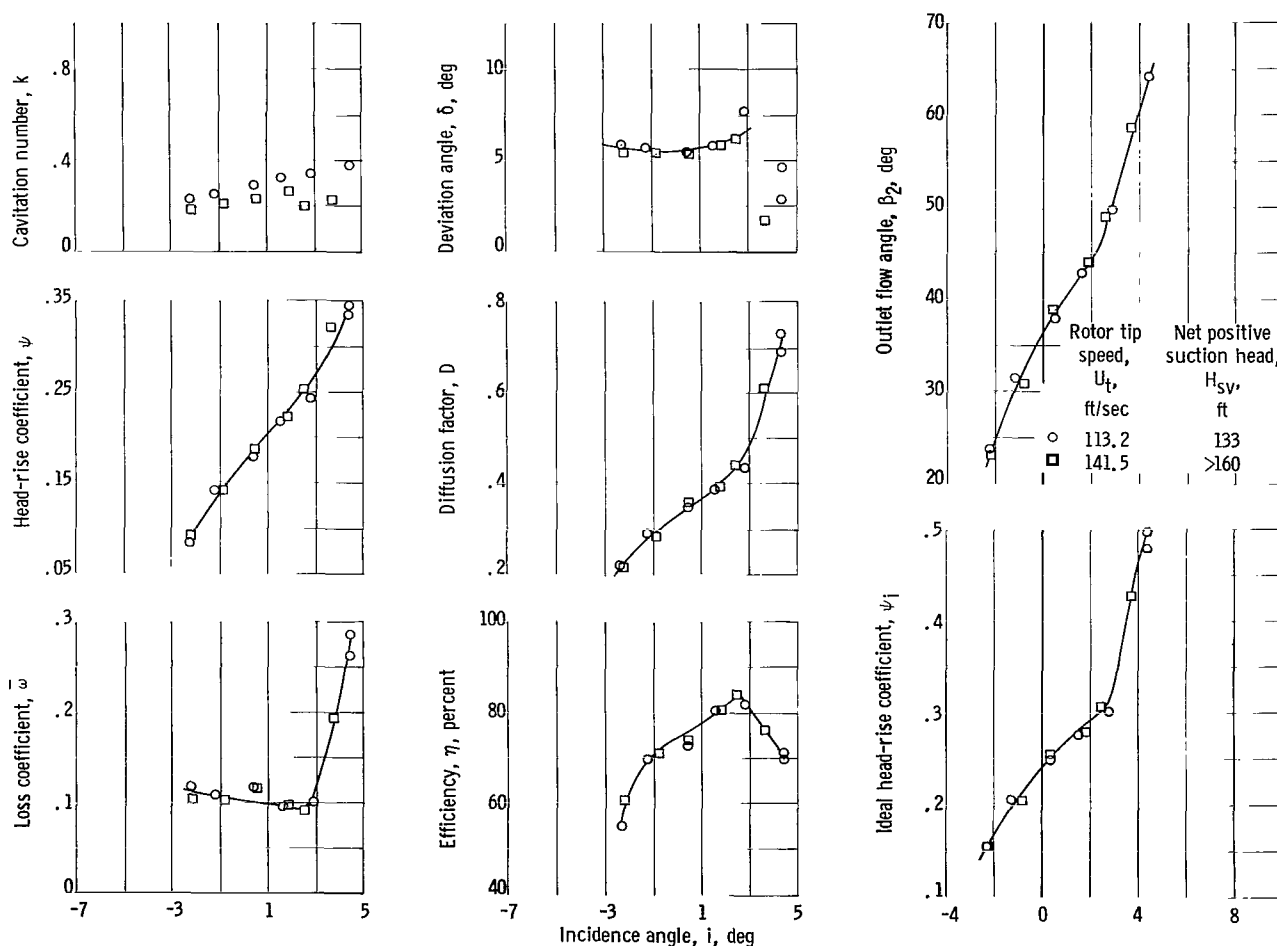
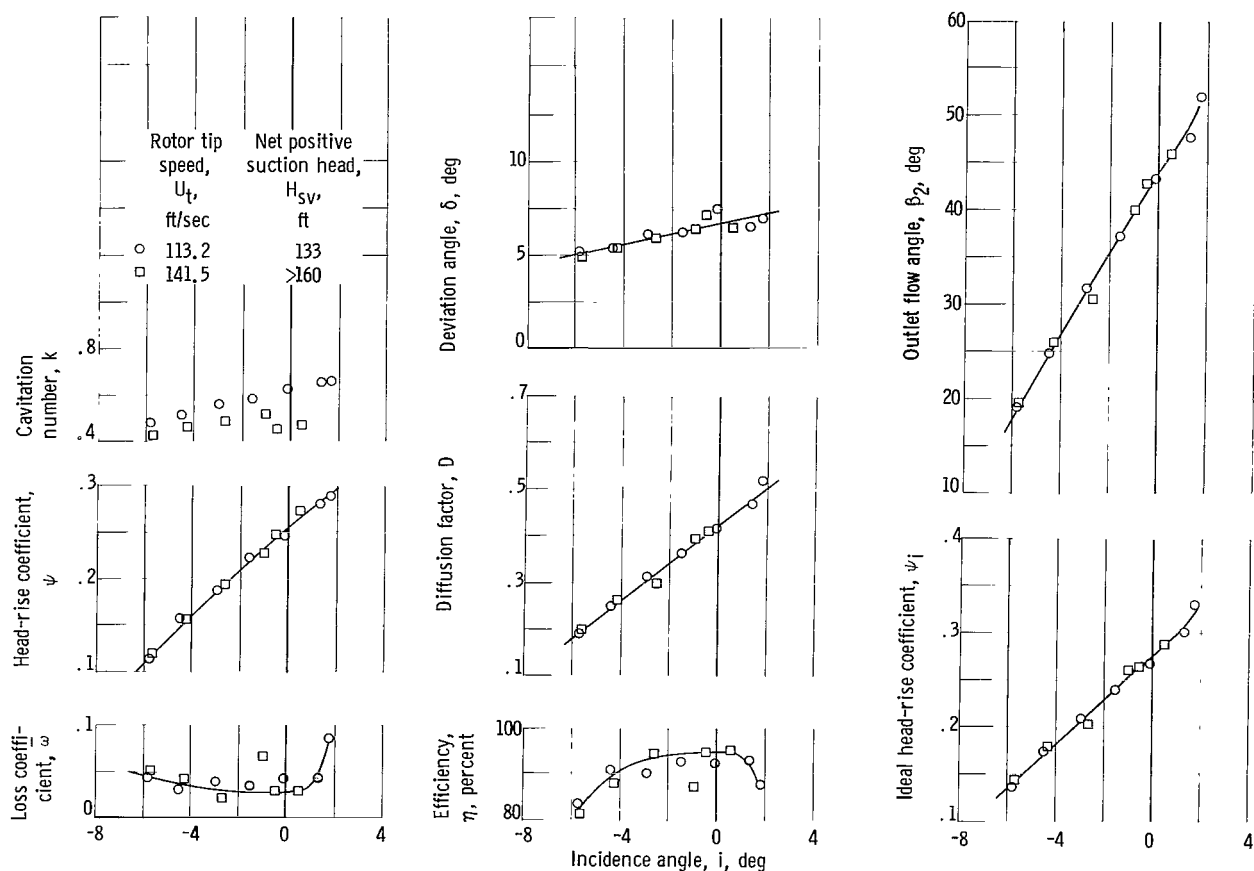(a) Radial position 1; rotor hub-tip radius ratio, 0.972.

Figure 7. - Rotor-blade-element performance characteristics for noncavitating conditions.

of attack at which no velocity peaks appeared on either blade surface as optimum or design. The cascade results showed the following related results:

(1) For a given cambered blade, the angle of attack operating range decreases as inlet-flow angle is increased.

(2) For operation at a 70° inlet-flow angle, the angle of attack operating range decreases as camber is increased. Also, the positive stall angle of attack approaches the design angle of attack more rapidly than the negative stall angle of attack.

The performance characteristics of the blade elements of this rotor appear to comply with the trends noted previously. Assuming that minimum loss and the most favorable blade surface velocity distributions occur at the same operating point (angle of attack), the small difference between the minimum-loss and positive blade stall operating points would indicate that the tip elements of this rotor are relatively highly loaded, even possibly approaching a limit loading condition for blade elements approximating this inlet angle range. The tip element (radial position 1 (RP 1)) incurred a D-factor of 0.44 at the minimum-loss operating point. By the standards set forth in reference 6 this would be
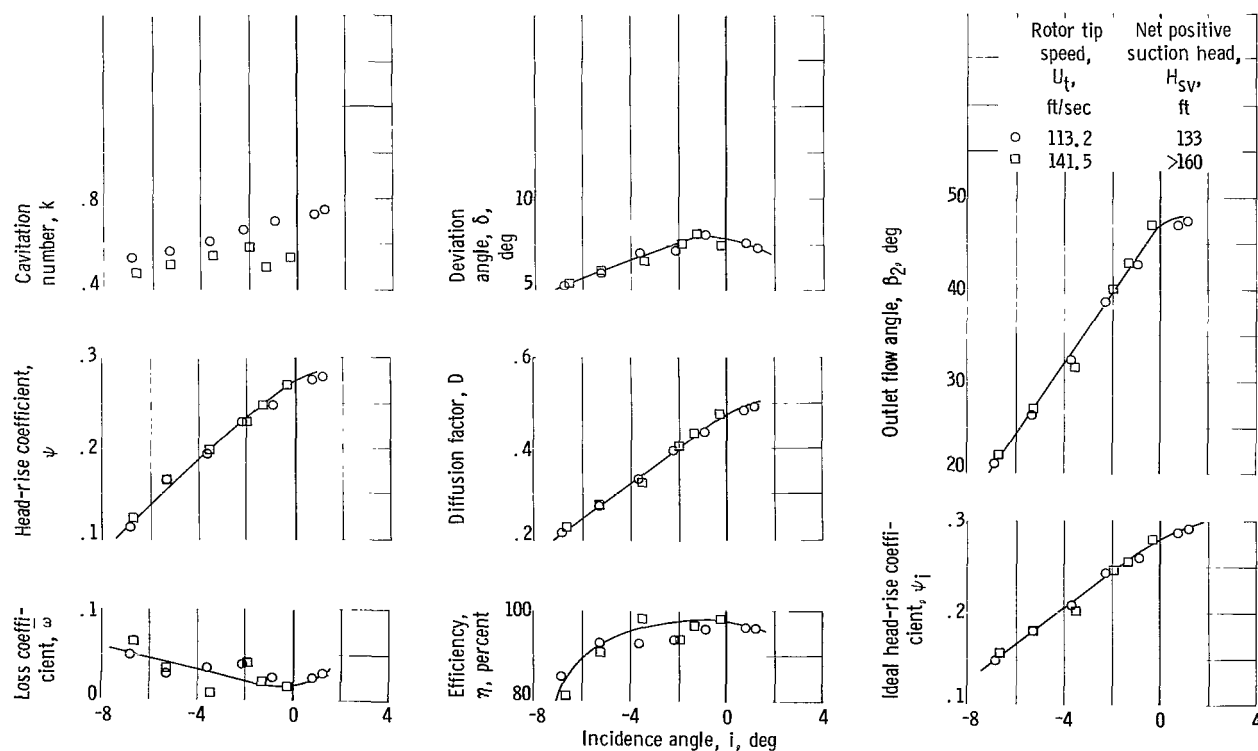

(b) Radial position 2; rotor hub-tip radius ratio, 0.906.

Figure 7. – Continued. Rotor-blade-element performance characteristics for noncavitating conditions.

12

considered a high loading for a tip element. The second element (RP-2) also achieved a D-factor of 0.44 at its minimum-loss operating point. While this value is not considered large for this element, the incidence angle difference between the minimum-loss and positive blade stall operating points also has increased slightly. Only performance trends are considered herein; hence, no attempt is made to assess effects of blade shape, solidity, maximum thickness, and other parameters on the observed values.

It is noted that, even at minimum-loss incidence angle, the loss in the tip measuring station (RP 1) is at least three times that measured at the other radial elements. Losses associated with casing boundary layer (RP 1 is 0.123 in. from outer wall), tip clearance flow, radial transport of blade boundary layer, and secondary flows probably all supplement the profile losses to some extent in this area. The very low loss levels ($\bar{\omega} < 0.02$) observed at RP 4 ($r/r_t = 0.794$) and RP 5 ($r/r_t = 0.728$) for the level of blade loading ($D > 0.5$) as compared to the level of loss coefficient observed in the tip region for lower levels of blade loading lead to speculation that radial transport of the low-energy blade boundary layer is occurring even with these short chord blades.

A method frequently used to establish the positive and negative stall points of a rotor (and thus define the usable flow ranges) is to assume that they occur when the loss is some multiple of the minimum-loss value. At the
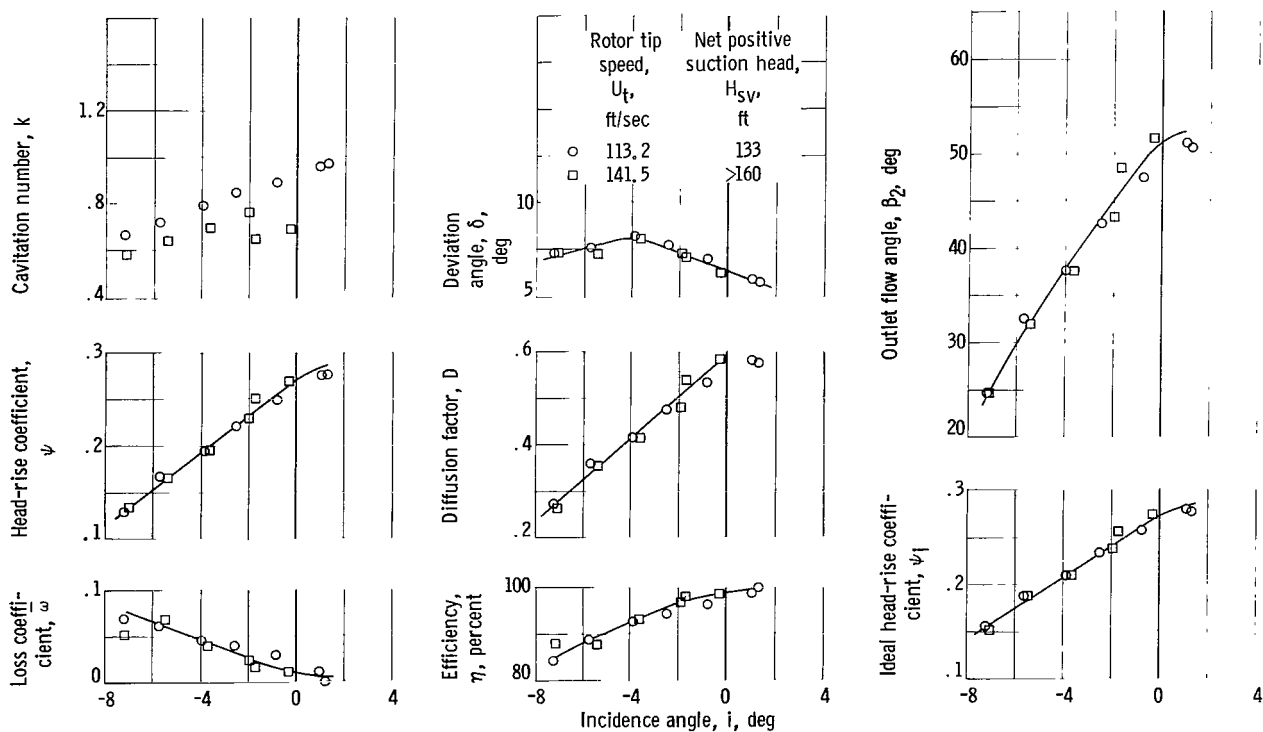

(c) Radial position 3; rotor hub-tip radius ratio, 0.850.

Figure 7. – Continued. Rotor-blade-element performance characteristics for noncavitating conditions.

13
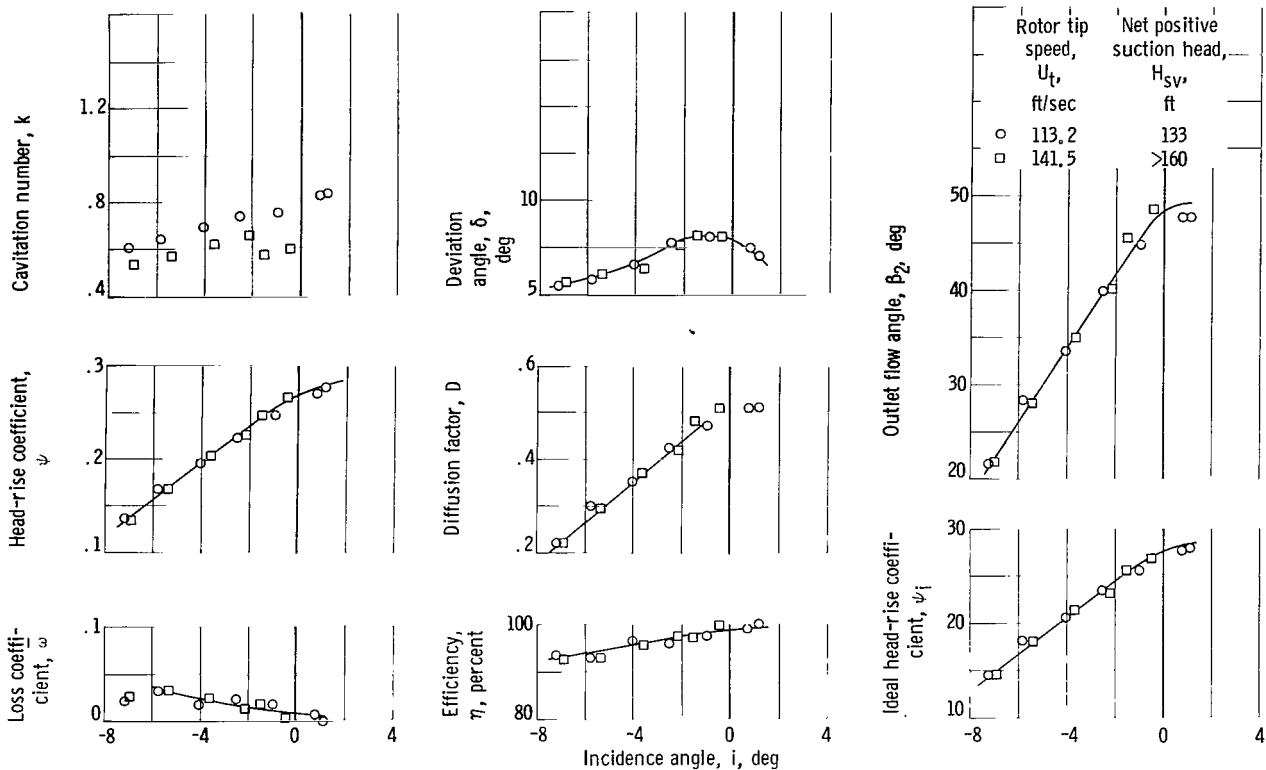
(d) Radial position 4; rotor hub-tip radius ratio, 0.794.

(e) Radial position 5; rotor hub-tip radius ratio, 0.728.

Figure 7. – Concluded. Rotor-blade-element performance characteristics for noncavitating conditions.

14

design-flow operating point, the tip element loss coefficient is approximately twice the minimum-loss value. Together with the sharp increase in loss, this indicates that separation of the blade surface boundary layer has occurred or is imminent. Apparently, at design conditions, then, the tip 10 percent of the blade height was operating in a stalled condition. All other elements were operating very close to their minimum-loss points, however; hence, the overall efficiency remained high.

At the lowest flow (highest incidence angle) at which survey data were taken, losses show a sharp increase (approximately three times) over the minimum-loss value at radial positions 1 and 2 (located at 10 and 30 percent of the passage height, respectively). Thus, in the operating range from design $\overline{\varphi} = 0.284$ to $\overline{\varphi} = 0.271$, the radial extent of blade stall conditions increased from at least 10 to 30 percent of the blade height. It was noted earlier that at $\overline{\varphi} < 0.271$ rig vibrations became excessive and prolonged operation was deemed inadvisable. It seems likely that complete blade stall occurred at these lower flow ($\overline{\varphi} < 0.271$) conditions.

While blade-element characteristic curves such as presented in figure 7 have been used primarily for establishing design-point data, they also provide the necessary values of deviation angle and loss coefficient for predicting off-design performance. At present their utility lies in direct application of the trends to similar blade rows. With the acquisition of additional data they may aid in the formulation of detailed off-design performance calculation procedures.

Comparisons with correlations of reference 1. - A specific purpose of this investigation was to consider the applicability of the design system for axial-flow air-compressor rotors presented in reference 1 to the design of axial-flow pumps. An operating condition commonly selected as the design point is the minimum-loss operating point. For each blade element minimum-loss levels and the difference between the observed pump rotor minimum-loss incidence (and deviation) angle and a value calculated from correlation of cascade data, $i_p - i_{2-D}$ and $\delta_p - \delta_{2-D}$ are compared with similar values recommended from air-compressor rotor tests $i_c - i_{2-D}$ and $\delta_c - \delta_{2-D}$. The following procedure was followed:

(1) From figure 7 values of minimum-loss coefficient and the corresponding incidence angle i_p, deviation angle δ_p, and diffusion factors for each element were selected.

(2) Fluid-flow angles were computed by using the values of (1) plus blade inlet and outlet angles.

(3) From flow angles and blade-element geometry (solidity, maximum-thickness-to-chord ratio, and camber angles) reference incidence and deviation angles based on two-dimensional cascade correlations (i_{2-D} and δ_{2-D}, respectively) were computed from methods of reference 1.

(4) Comparisons of measured rotor performance parameters at reference conditions with the computed values from (3) are presented in the form $i_p - i_{2-D}$,

$\delta_p - \delta_{2-D}$, and $\bar{\omega} \cos \beta_2/2\sigma$. The observed values for each element are shown on table II together with correction factors for incidence and deviation angles obtained from numerous air compressor tests.

TABLE II. - COMPARISON OF MEASURED MINIMUM-LOSS PERFORMANCE PARAMETERS

WITH THOSE COMPUTED FROM DESIGN RULES OF REFERENCE 1

Radial position, RP	Approximate percent passage height	Minimum-loss performance parameters			Correction factors				Loss coefficient, $\dfrac{\bar{\omega} \cos \beta_2}{2\sigma}$	Diffusion factor, D
		i_p, deg	$\bar{\omega}$	δ_p, deg	$i_p - i_{2-D}$, deg	$i_c - i_{2-D}$, deg	$\delta_p - \delta_{2-D}$, deg	$\delta_c - \delta_{2-D}$, deg		
1	10	2.4	0.092	6.4	2.3	-2.5	2.1	-1.5	0.0159	0.441
2	30	0.4	0.030	6.8	2.3	-2.0	0	-1.0	0.0060	0.440
3	50	0.0	0.015	7.5	2.3	-1.6	-0.3	-0.5	0.0022	0.479
4	70	1.1	0.005	7.1	3.5	-1.0	-1.4	0.2	0.0012	0.511
5	90	1.3	0.007	5.7	3.4	-0.7	-3.4	1.0	0.0017	0.575

While the data presented in table II refer only to a minimum-loss design point, they do provide sufficient evidence that some extension and possibly modification of certain parts of the design system of reference 1 are necessary for accurate prediction of reference incidence and deviation angles for axial flow pumps. The performance results of a similar type rotor reported in reference 3 led to the same conclusion. A more detailed discussion applying the experimental results from this rotor to an evaluation of the design system follows in the section Evaluation of Blade Design System.

In figure 8 the loss-coefficient parameters at minimum-loss incidence angle for two rotors operating in water are compared with similar results obtained from single-stage axial-flow air-compressor rotors. The shaded area represents the region in which tip loss parameters fell. The additional rotor data plotted on figure 8 was taken from reference 3 where similar comparisons were made.

The loss parameter plotted in figure 8 is a simplified form of the wake momentum thickness developed in reference 7. This theoretical loss analysis (reported in ref. 7) establishes blade-wake momentum thickness as the primary wake characteristic descriptive of the total pressure defect resulting from boundary layer flow around a blade element and establishes relations for estimating this blade profile loss. Thus, wake momentum thickness represents a generalized loss parameter that is a function only of individual blade wakes and independent of the blade row geometry (solidity and air angles). The establishment of a generalized loss parameter is further investigated in reference 8 by an analysis of experimental loss characteristics of low-speed air cascade sections in terms of wake momentum thickness and a blade velocity diffusion factor. In reference 1 the simplified wake momentum thickness expres-
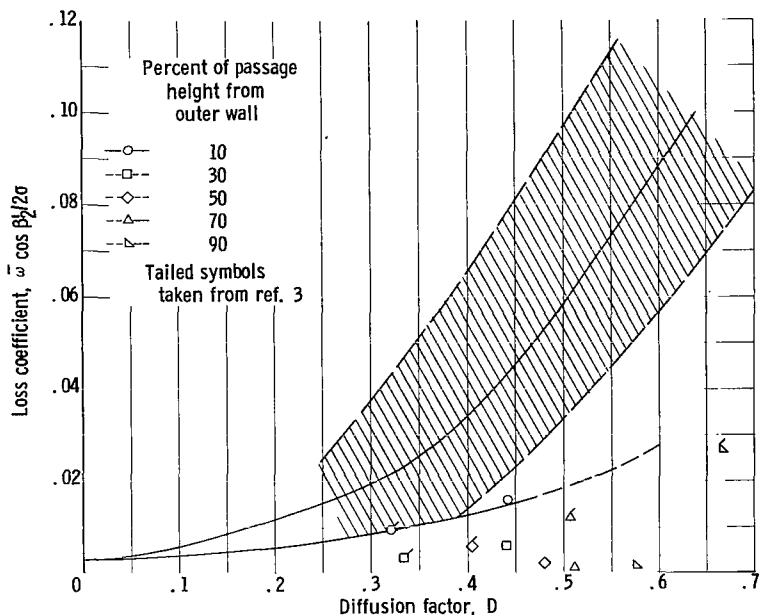
Percent of passage
height from
outer wall

—○— 10
--□-- 30
-◇-- 50
--△-- 70
--▷-- 90

Tailed symbols
taken from ref. 3

Loss coefficient, $\bar{\omega} \cos \beta_2'/2\sigma$

.12 .10 .08 .06 .04 .02 0

Diffusion factor, D
0 .1 .2 .3 .4 .5 .6 .7

Figure 8. – Comparison of measured axial-flow pump results at minimum-loss incidence angle with correlations of reference 1.

sion is correlated with losses measured in the three-dimensional environment of single-stage compressor rotors.

A specific explanation for the generally lower levels of the wake momentum thickness expression for pump rotors as compared to air-compressor rotors is not readily apparent. Blade-geometry features (blade shape, camber, solidity, aspect ratio, blade thickness to chord ratio, etc.) are similar. Also, the levels of loss coefficient $\bar{\omega}$ for a given level of blade loading (D-factor) at the various blade elements are close. The one significant difference is the high flow angles of the pump rotor as compared to those encountered in the correlation of the cascade and air compressor rotor data. At present, no generalization will be attempted on the basis of the performance of this limited number of rotors other than to recommend caution in applying this loss parameter to blades with high outlet blade angles.

Cavitating Performance

The type of rotor whose performance is presented herein is ordinarily not expected to operate in an environment conducive to cavitation. Its high hub-tip ratio and level of loading are typical of the type of rotor used in the high-pressure portion of a multistage axial-flow pump. In order to know the level of inlet head needed before such a rotor can be used, however, a minimum amount of cavitation performance was obtained and is presented. Although all the data taken are presented, a discussion of the cavitating performance is limited to a few significant features.

Overall performance. – The overall performance is presented in figure 9 in terms of mass-averaged values of head-rise coefficient $\bar{\psi}$, efficiency $\bar{\eta}$, and flow coefficient $\bar{\varphi}$. Noncavitating performance is also shown for comparison.

The overall performance is discussed in reference 4, and the results are summarized by the following:

(1) Initial effects of cavitation on performance of this rotor are felt at an H_{sv} of approximately 116 feet. The dropoff in performance is observed
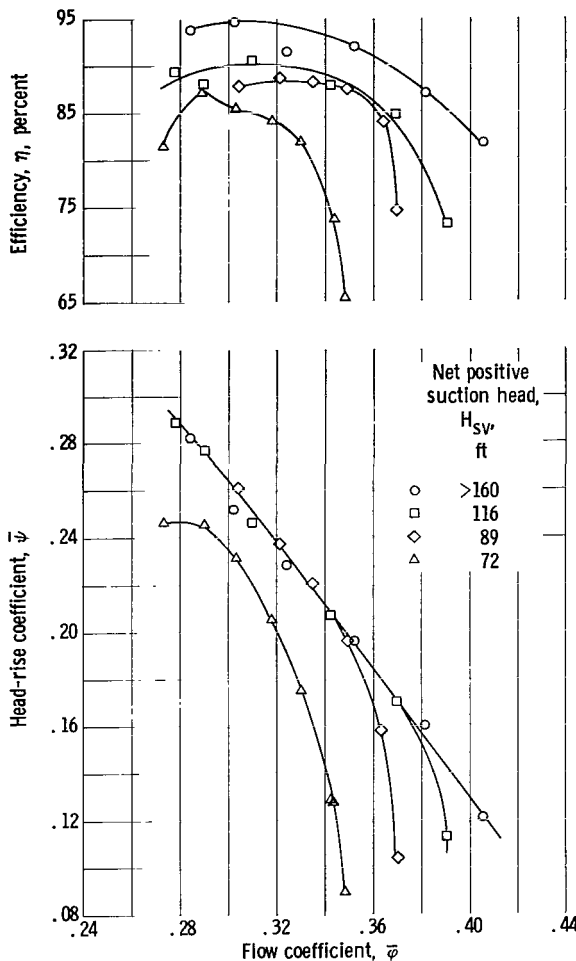
Figure 9. - Overall performance for cavitating and non-cavitating conditions.

Net positive suction head, H_{SV}, ft
o >160
□ 116
◇ 89
△ 72

only at high flow at these inlet conditions.

(2) At design-flow coefficient, cavitation did not affect rotor head rise until an $H_{SV} < 89$ feet was reached.

(3) Rotor efficiency $\bar{\eta}$ was decreased from the noncavitating values at all inlet pressures below an H_{SV} of 116 feet.

Blade-element performance. - Figure 10 presents the radial distributions of flow and blade-element performance for an H_{SV} of 72.5 feet and three inlet-flow coefficients covering the range of operation. These flow conditions represent suction specific speeds of 9009 ($\bar{k} = 0.148$) to 10,220 ($\bar{k} = 0.100$) for inlet-flow coefficients of 0.273 and 0.348, respectively. To observe the effects of cavitation on performance, the distributions of figure 10 should be compared with the curves of figure 6 (noncavitating performance). With the exception of cavitation number k the inlet-flow parameters at the two modes of operation are similar, indicating that inlet-flow geometry is being maintained. Comparison of the outlet-flow conditions and element performance parameters indicate the following general effects and radial variations:

(1) Both the ideal and actual head coefficients are similar, but under cavitating conditions ($H_{SV} = 72.5$ ft) the level of performance is decreased.

(2) Loss-coefficient plots show the same high values of $\bar{\omega}$ in the tip region compared to other radial locations. Also, the level of loss increases with occurrence of cavitation.

(3) The general trend of deviation angle is to increase as H_{SV} is lowered (cavitation increasing).

(4) Differences in radial equilibrium requirements are reflected in the radial distributions of flow coefficient. Radial equilibrium requirements vary as cavitation (or change in mode of operation) affect the radial gradients of the element performance parameters. At the high flows ($\bar{\varphi} \approx 0.350$) the radial distribution of axial velocity under cavitating ($H_{SV} = 72.5$ ft)
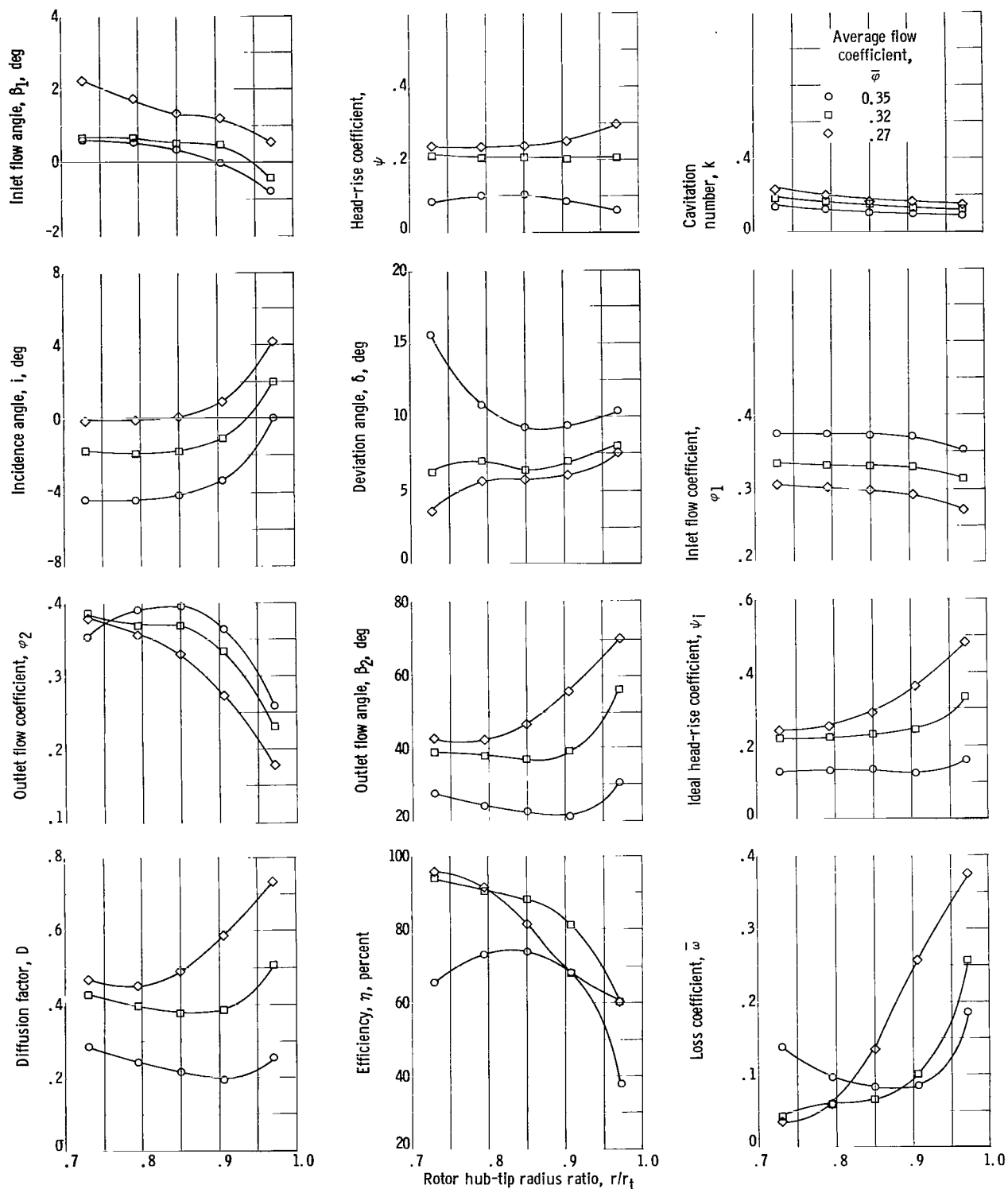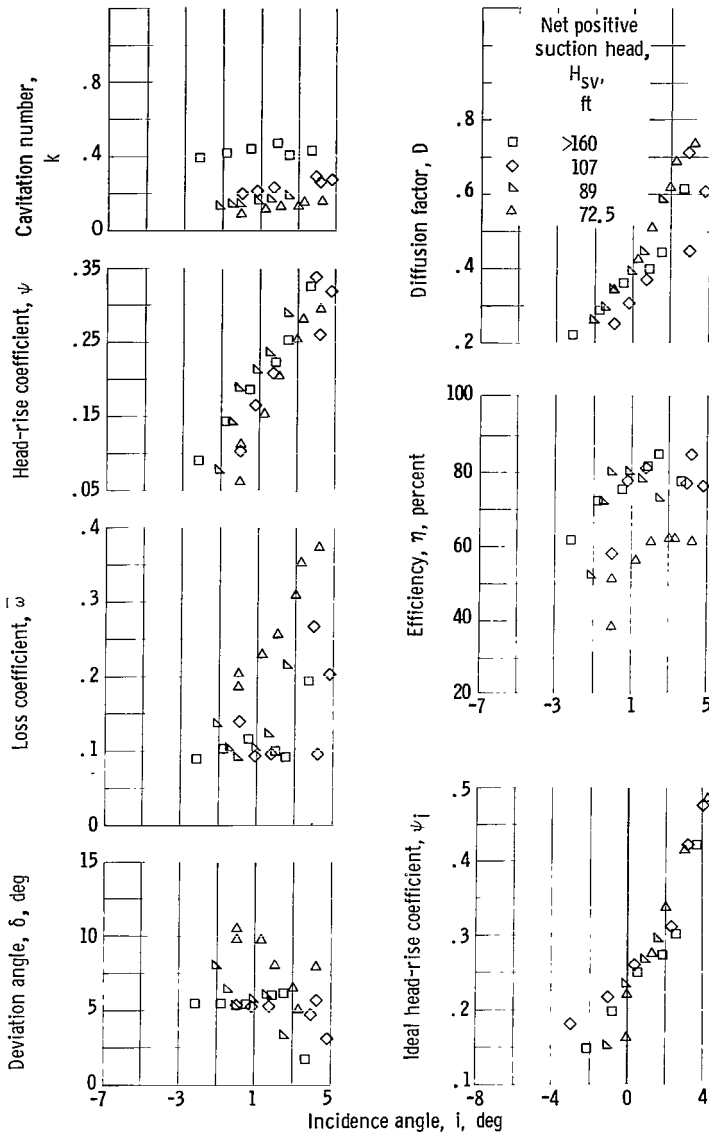
18

Figure 10. – Radial distributions of flow and blade-element performance parameters under cavitating conditions. Rotor tangential velocity at tip, 141.5 feet per second; net positive suction head, >160 feet.

19

(a) Radial position 1; rotor hub-tip radius ratio, 0.972.

Figure 11. – Blade-element performance characteristics for cavitating and noncavitating conditions. Rotor tip speed, 141.5 feet per second.

and noncavitating ($H_{SV} > 160$ ft) flow are surprisingly close. At lower flow coefficients it appears the cavitation effects are more severe and comparisons would not be as favorable. In summary, cavitation would affect the level of performance of the rotor and present matching problems in a succeeding blade row as well.

Figure 11 presents the performance of the individual blade elements by showing the variations of selected performance parameters with incidence angle. Both noncavitating and cavitating data are recorded.

The same general effects of cavitation on performance noted previously (comparison of figs. 6 and 10) are again evidenced by the plots of figure 11. One additional result of cavitation indicated by these curves is that it appeared to decrease the low-loss incidence angle range.

Radial Equilibrium

The design of this rotor assumed that simple radial equilibrium (neglecting effects of radial accelerations) defined by

$$\frac{\partial h}{\partial r} = \frac{V_\theta^2}{gr} \qquad (1)$$

adequately expresses the radial gradient of outlet-flow conditions. Figure 12, which is reproduced from reference 4, compares measured axial velocity distributions with those computed using the simple radial equilibrium expression. The plots both validate the design assumption and indicate that the simple radial equilibrium expression would be applicable under all flow conditions, both cavitating and noncavitating, experienced in these rotor tests.

20
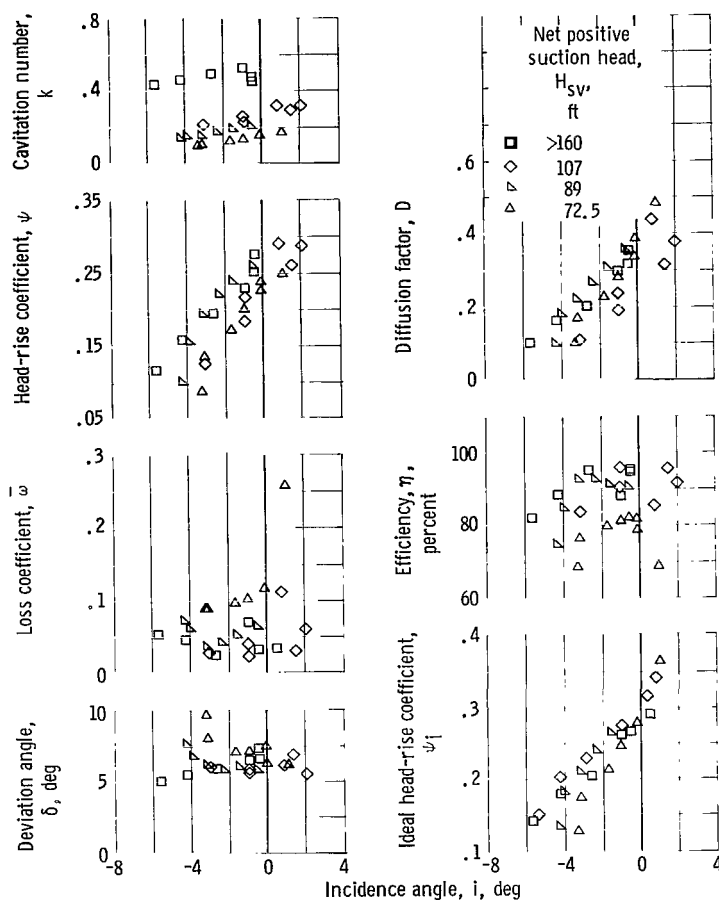
(b) Radial position 2; rotor hub-tip radius ratio, 0.906.

Figure 11. – Continued. Blade-element performance characteristics for cavitating and noncavitating conditions. Rotor tip speed, 141.5 feet per second.

Evaluation of Blade

Design System

The design whose performance is reported herein is characterized by high inlet-relative-flow angles, radially constant energy addition, and high hub-tip radius ratio. In the following discussion the performance results from this rotor and experiences during the formalizing of the design are examined with reference to general application of the blade design system.

The utility of a design system is judged on its ability to produce blade rows that provide

(1) The desired level of head rise and an acceptable efficiency at the design flow

(2) Adequate stable operating flow margin on either side of the design flow based on considerations of startup, acceleration, and engine throttle ability requirements

This pump blade design system for axial-flow stages is closely patterned after the blade design system for axial-flow air compressors reported in reference 1. The equations take the form

$$\varphi^{\circ} = \Delta\beta' - i_p + \delta_p = \Delta\beta' - \left[i_{2\text{-}D} + (i_p - i_{2\text{-}D})\right] + \left[\delta_{2\text{-}D} + (\delta_p - \delta_{2\text{-}D})\right] \quad (2)$$

where $i_{2\text{-}D}$ and $\delta_{2\text{-}D}$ are suggested design values of incidence and deviation angles, respectively, obtained from correlations of two-dimensional low-speed air-cascade performance data. Rules for predicting these values as a function of inlet-flow angle, blade solidity, and maximum blade thickness are presented in reference 1. The $i_p - i_{2\text{-}D}$ and $\delta_p - \delta_{2\text{-}D}$ represent adjustments, or correction factors, for the effects of operating in a three-dimensional environment.

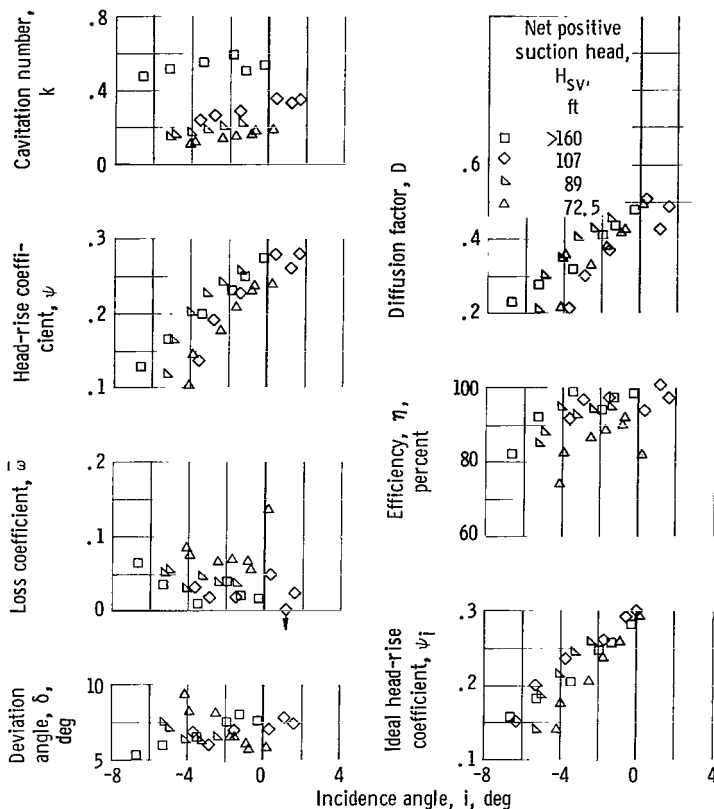Potential difficulties in applying this system could arise in several areas:

(c) Radial position 3; rotor hub-tip radius ratio, 0.850.

Figure 11. - Continued. Blade-element performance characteristics for cavitating and noncavitating conditions. Rotor tip speed, 141.5 feet per second.

(1) In general, pumps utilize higher inlet-relative-flow angles than air compressors. In many pump designs, including the design reported herein, a number of elements of the pump in the tip region will have inlet angles above the maximum values covered in cascade investigations ($\beta_1 < 70^\circ$). In this high inlet angle range, the design system curves have steep and changing slopes; consequently, extrapolation is uncertain and the accuracy of the calculated i_{2-D} values is also unknown.

(2) It is not known whether the three-dimensional correction factors $i_c - i_{2-D}$ and $\delta_c - \delta_{2-D}$ empirically determined for air compressors may be applied directly.

Optimum design-point performance would be obtained if all the rotor elements were operating at their minimum-loss incidence angles at the design flow. Blade-element performance indicated that the measured rotor minimum-loss incidence angles were higher than the calculated two-dimensional values i_{2-D} by 2.3° (tip) to 3.4° (hub). Thus, $i_p - i_{2-D}$ in equation (2) should be positive. By contrast, these correction factors $i_c - i_{2-D}$ recommended for low inlet Mach number air-compressor rotors are negative (see table II).
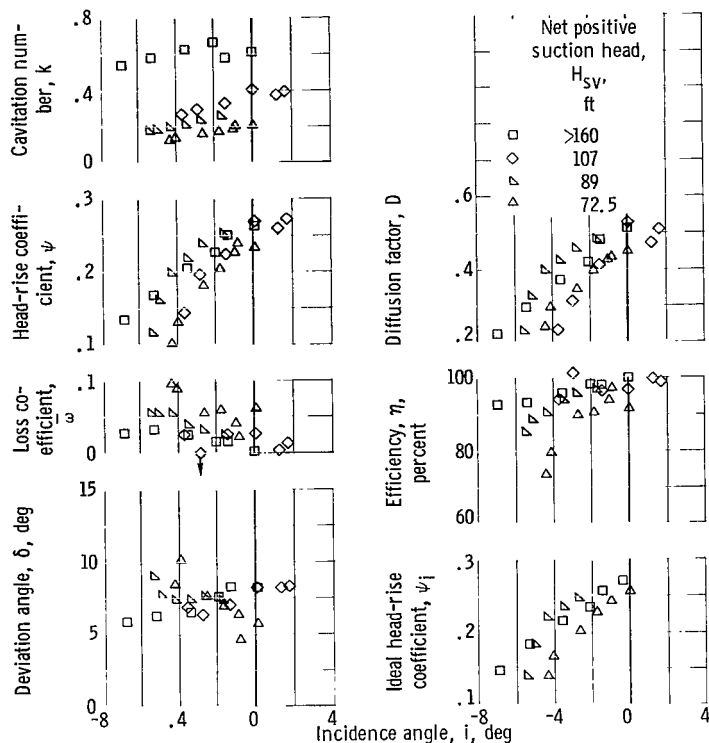
If it is assumed that the blade-element performance curves obtained from this rotor are somewhat typical of those for this type of rotor design, a significant feature is that the minimum-loss incidence angle occurs very close to the element stall operating incidence (considered herein as effectively occurring when $\overline{\omega} = 2\overline{\omega}_{m,1}$). If an increase in stable operating flow range between design and blade stall is desired, the design incidence would be moved toward the high flow side of the minimum-loss incidence by using lower values of $i_p - i_{2-D}$ than those noted previously for minimum-loss point. The blade-element characteristics indicate that only a small penalty in increased loss coefficient would result from locating the design point at an incidence angle slightly lower than the minimum-loss incidence angle.

It is thus indicated that a preferable design flow operating point for a

Figure 11. - Continued. Blade-element performance characteristics for cavitating and noncavitating conditions. Rotor tip speed, 141.5 feet per second.

(d) Radial position 4; rotor hub-tip radius ratio, 0.794.

rotor row of this type would utilize an incidence angle equal to or slightly larger than the calculated two-dimensional value; that is, $i_p - i_{2-D} = 0$ or slightly positive. Consequently, the calculated two-dimensional deviation angles δ_{2-D} are compared with measured rotor deviation angles in the range of incidence angles $i_{2-D} < i < i_{2-D} + 2^\circ$.

In the region from 30 to 70 percent of passage height from the tip (RP 2, 3, and 4), the measured rotor deviation angles are within approximately 0.5° of the calculated two-dimensional values. Thus, over this range of blade height, the calculated two-dimensional values would suffice, or $\delta_p - \delta_{2-D} = 0$. In the blade tip region the observed rotor deviation angles were slightly higher than the calculated two-dimensional values, or $\delta_p - \delta_{2-D} \a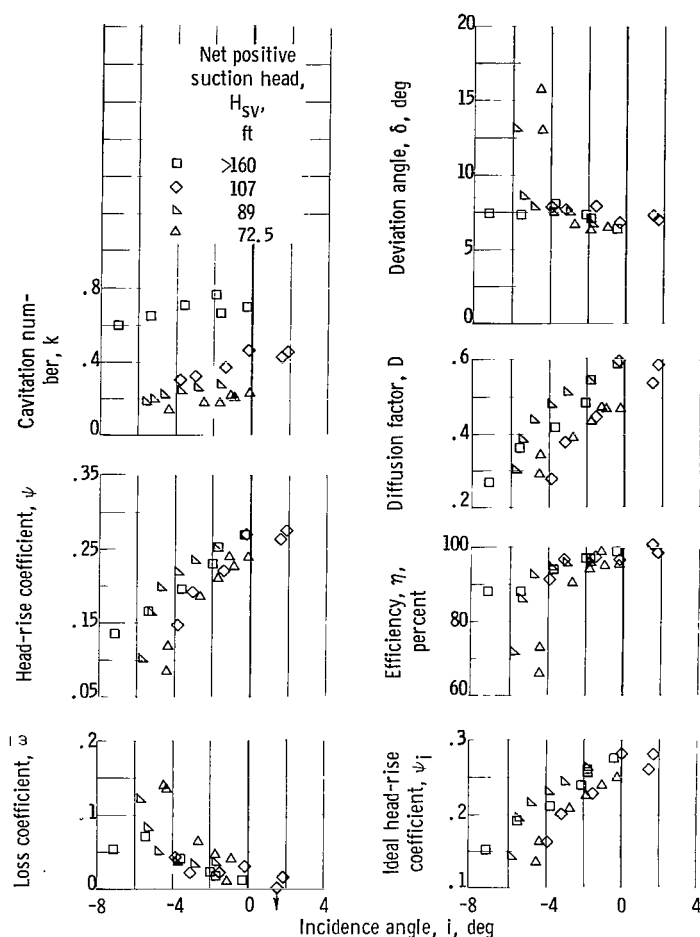pprox + 1.5$. In the blade hub region the reverse trend was observed; that is, $\delta_p - \delta_{2-D} \approx -2.5$. A satisfactory explanation to generalize the hub value result is not apparent other than to note that it occurs in the region where secondary flows and three-dimensional effects are prevalent. The very low loss level measured in the hub region and the steep gradient of loss in the blade tip region are an indication that secondary flows are significant. In contrast, the correction factors determined for axial-flow air compressors $\delta_c - \delta_{2-D}$ showed slightly negative values in the tip region, values near zero at the mean radius and slightly positive values in the hub region.

An important design consideration is the magnitude and radial distribution of loss. The air compressor design methods presented in reference 1 suggest the use of a generalized loss parameter $\bar{\omega} \cos \beta_2'/2\sigma$. As noted previously, however, when the measured pump rotor losses are expressed in this form, they do not correlate with the air-compressor results. At present this disagreement is attributed to the effects of the relatively high fluid-inlet angle.

A comparison of the measured pump rotor loss coefficients and diffusion factors at minimum-loss incidence angle with cascade and air-compressor results as reported in reference 5 indicates the following:

(e) Radial position 5; rotor hub-tip radius ratio, 0.728.

Figure 11. – Concluded. Blade-element performance characteristics for cavitating and noncavitating conditions. Rotor tip speed, 141.5 feet per second.

(1) In the tip region the loss coefficient was significantly higher than the value indicated from cascade results, but it did fall inside the band of data obtained from air-compressor rotor tests.

(2) At the mean radius the loss coefficient was slightly lower than the cascade value for the same D-factor and among the lower level of values measured in air-compressor rotor tests.

(3) In the hub region the loss coefficient was significantly lower than the cascade value and among the lowest values measured in air-compressor tests.

The radial distribution of loss coefficients and the comparison with cascade values for similar D-factor levels of loading indicate the presence and importance of secondary flows. For the present, secondary flow effects will be accommodated by considering the loss parameter as a function of blade loading (D-factor) and radial location. Some insight into the severity of secondary flows occurring in a design may be obtained from a simple analysis (notes from Penn. State Univ. seminar, 1958) that indicates that the quantity of flow involved in secondary motions is

(1) Directly proportional to the square of the circumferential projection of a blade

(2) Inversely proportional to the angle between the inlet relative flow (or blade inlet camber line) and the circumferential direction

The use of these two parameters provides some qualitative direction to the selection of a radial gradient of loss.

The results obtained in this investigation point out the necessity of accurately defining the inlet velocity diagrams for a design with this level of loading and inlet angle. In this case the outer casing boundary layer caused the tip-element flow velocity to fall below its anticipated design value and

24

Average flow coefficient, $\bar{\varphi}$ | Average rotor head-rise coefficient, $\bar{\psi}$

0.405 | 0.121

70

60

50

.352 | .196

60

50

40

Axial velocity at rotor exit, $V_{2,z}$, ft/sec

.302 | .251

45

35

.284 | .284

45

35

.7 .8 .9 1.0

Rotor hub-tip radius ratio, r/r_t

(a) Noncavitating condition.

Average flow coefficient, $\bar{\varphi}$ | Average rotor head-rise coefficient, $\bar{\psi}$

0.348 | 0.090

65

55

45

35

.318 | .205

60

50

40

30

.273 | .246

55

45

35

25

.7 .8 .9 1.0

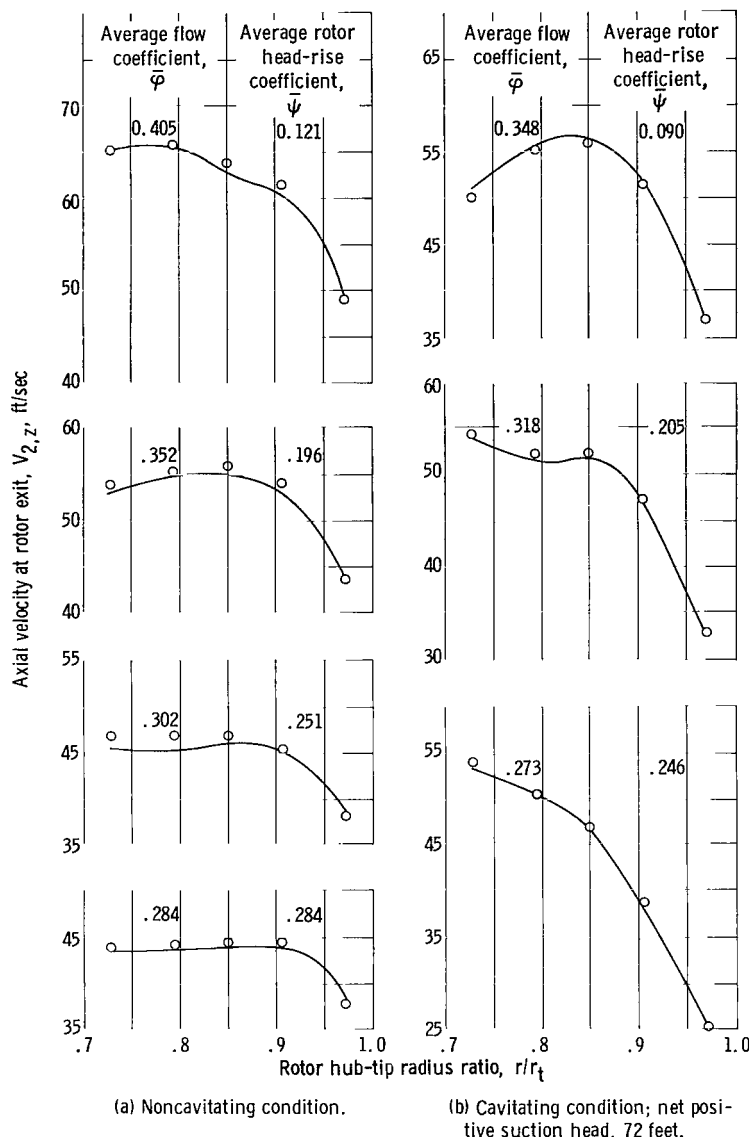(b) Cavitating condition; net positive suction head, 72 feet.

Figure 12. - Comparison of measured axial velocity distribution behind rotor with axial velocity distribution calculated by simple radial equilibrium.

the blade element to operate at a higher than design incidence value. This resulted in premature stalling flow conditions in the tip region and was partly responsible for the small flow margin between design flow and the positive blade stall point.

Predicting the effects of casing boundary layer on the inlet flow distribution is very difficult, and if the boundary layer velocity gradient could be accurately predicted, it could not be incorporated into the blade design system because of the prohibitive amounts of blade twist involved. Perhaps the only correction that can be applied in this area is to anticipate the boundary layer effects and allow for them in the blade design method, primarily in the use of lower values of $i_p - i_{2-D}$. Improved methods of calculating radial gradients of inlet velocity due to streamline curvature, however, should be applied. Reference 8 discusses this problem in more detail.

In the design of this rotor as discussed in reference 4 it was noted that modifications to the calculated blade parameters in the tip region were made. The necessity for this becomes clear in the following discussion of the sensitivity of the blade camber design equation at high inlet-flow angles to variations in the correction factors $i_p - i_{2-D}$ and $\delta_p - \delta_{2-D}$. These latter factors are the type of information that must be obtained from rotor performance results of investigations such as reported herein and in reference 3 or from low-speed air-compressor rotor tests. To demonstrate this sensitivity, the design velocity diagrams and specified blade shape, solidity, and blade thickness values for this rotor were applied to the blade camber design equation for four different sets of assumptions. Calculated design values of blade camber angle, incidence, and deviation angles for the tip, mean, and hub blade elements are listed in the following table:

Part	Rotor hub-tip radius ratio, r/r_t	Three-dimensional correction factors, $i_p - i_{2-D}$, deg	$\delta_p - \delta_{2-D}$, deg	Camber angle, φ^o, deg	Incidence angle, i, deg	Deviation angle, δ, deg
1	1.0	3.0	0	-11.6	10.7	-2.8
	.85	↓	↓	19.8	.5	7.8
	.70	↓	↓	27.6	1.2	9.3
2	1.0	0	0	0.3	3.0	1.4
	.85	↓	↓	28.0	-5.1	10.4
	.70	↓	↓	33.7	-3.2	10.9
3	1.0	3.0	-1.75	-18.6	13.4	-7.0
	.85	↓	-.50	18.4	.9	6.9
	.70	↓	1.50	30.7	.5	11.6
4	1.0	0	1.50	6.2	0.7	5.1
	.85	.5	-.50	25.2	-3.7	9.1
	.70	1.0	-2.50	26.6	-.6	6.5

Part 1 lists the initial values of three-dimensional correction factors used in the design of this rotor. At the tip element, where the tip inlet-relative-flow angle necessitated extrapolating certain curves to calculate i_{2-D} and δ_{2-D}, negative values of camber and deviation angles and an unusually high value of design incidence angle were obtained as shown. The tip-element blade section was arbitrarily changed as noted in reference 4.

Part 2 presents the blade parameters calculated for this design if no corrections are made for prediction of three-dimensional effects.

Part 3 shows the blade parameter values when the deviation angle correction $\delta_p - \delta_{2-D}$ as deduced from air-compressor tests is used; that is,

$$\delta_p - \delta_{2-D} = \delta_c - \delta_{2-D}$$

The 3° incidence angle correction factor was used in order that comparisons with table I (see p. 3) values could be made.

Part 4 lists the values of $i_p - i_{2-D}$ and $\delta_p - \delta_{2-D}$ that would probably be recommended for application in the blade design equation for a redesign of this rotor on the basis of present information. The $i_p - i_{2-D}$ variation was selected to provide flow margin between the design and positive blade stall operating points. In part 4 the blade parameters are computed based on the existing velocity diagram design values. A true redesign would suggest certain changes in the velocity diagram design that in turn would be reflected in the blade design values.

The fact that the calculations give negative camber and deviation angles indicates the need for a careful evaluation of the design system for use at high inlet-flow angles. The combination of high inlet-flow angle, small required fluid turning angles, and minimum allowable blade thicknesses found for the typical tip element make this region of the blade especially sensitive.

Comparisons of the values of parts 1 to 4 illustrate the sensitivity of the blade design equations to variations of the correction factors for incidence and deviation angle. They also indicate the need for precise measure-

ments during testing and careful definitions of reference angles from data plots.

Finally, the performance characteristics of this rotor together with the data of reference 6 indicate that at high values of both inlet-flow angle and loading small changes can result in significant variations in blade design or blade performance parameters. Consequently, in blade rows of this type, if acceptable levels of design point performance and blade stall margin are to be obtained, careful attention should be made to all details of the design.

SUMMARY OF RESULTS

An axial-flow-pump rotor with a 0.7 hub-tip ratio and design D-factors of 0.43 and 0.70 at the tip and hub, respectively, was tested in water. The following summarize the principal results observed from the rotor blade element performance:

Under noncavitating conditions

1. At design flow a comparison of the blade element performance with design values indicates the following:

    (a) Inlet axial velocity was higher than design except in the tip region, where it was lower than design (probably because of effects of outer casing boundary layer). This forced the tip element to operate very close to a blade stall condition.

    (b) Measured losses were lower than design except in the tip region, where they were considerably higher than the predicted design values.

    (c) Excluding the tip region, energy addition was lower than design but combined with the lower-than-design losses to produce a close-to-design head-rise coefficient. In the tip region the energy addition was higher than design and produced a higher-than-design head-rise coefficient (in spite of higher-than-design losses) but at a lower-than-design efficiency.

2. For this specific rotor geometry and level of loading, a typical loss-coefficient against incidence angle characteristic showed the following:

    (a) Minimum loss, where defined, occurred over a very narrow flow range.

    (b) Flow (or incidence angle) margin between minimum-loss operating condition and positive stall point (defined as point at which the loss coefficient was twice the minimum value on the high incidence (low-flow) side of the minimum-loss operating point) was very small.

    (c) Gradual increase in loss coefficient as the flow was varied from the minimum-loss value to higher flows (lower incidence angle).

3. A comparison of the measured results with those predicted from the design rules of reference 1, and interpretation of these results indicate that

(a) Application of the design rules to designs with inlet-flow angles outside the range covered by the two-dimensional air-cascade data used to formulate the design procedure is dangerous. Additional cascade data at the higher inlet-flow angles would be desirable.

(b) The blade design equations are very sensitive to small angle variations at high inlet-flow angles. This indicates the need for precise measurements and careful interpretation of the data from investigations of this type of pump rotor.

(c) With the type of loss coefficient - incidence angle characteristic measured for this type blade, considerations of flow margin between design and positive blade stall points indicate that the minimum-loss operating condition may not be a desirable design point for many applications.

(d) Significant differences between reference blade deviation angles obtained from two-dimensional cascade results and three-dimensional rotor tests occurred only in hub and tip regions where loss levels indicated secondary flow effects were significant.

Under cavitating conditions

1. At a rotor tip speed of 141.5 feet per second the effects of cavitation on rotor performance are first noted at a net positive suction head of 116 feet. This corresponds to an average cavitation number of approximately 0.191.

2. Cavitation generally affects rotor performance in the following ways:

(a) Increases losses

(b) Decreases energy addition

(c) Decreases low-loss operating range

Lewis Research Center
    National Aeronautics and Space Administration
        Cleveland, Ohio, June 23, 1964

28

APPENDIX A

SYMBOLS

c   blade chord, in.

D   diffusion factor

g   acceleration due to gravity, 32.17 ft/sec^2

H   total head, ft

H_{sv} net positive suction head, ft

ΔH head rise, ft

h   static head, ft

h_v vapor head, ft

i   incidence angle, deg

k   cavitation number

N   rotative speed, rpm

Q   flow rate, gal/min

r   radius, in.

U   rotor tangential velocity, ft/sec

V   fluid velocity, ft/sec

β flow angle, angle between direction of flow and axial direction, deg

γ blade setting angle, angle between chord line and axial direction, deg

δ deviation angle, deg

η efficiency, percent

κ blade angle, angle between tangent to blade mean camber line and axial direction, deg

σ blade solidity, c/s

φ flow coefficient

φ^o blade camber angle, $\kappa_1 - \kappa_2$, deg

ψ head-rise coefficient

$\bar{\omega}$ rotor relative total head-loss coefficient

Subscripts:

c   parameter obtained from air-compressor stage investigations

h   hub

i   ideal

m   measured

max   maximum

p   parameter obtained from pump-stage investigations

t   tip

z   axial direction

θ tangential direction

2-D   parameter obtained from two-dimensional air-cascade investigation

1   measuring station at rotor inlet

2   measuring station at rotor outlet

Superscripts:

$-$ averaged value

$'$ relative to rotor

APPENDIX B

EQUATIONS

Blade Element Equations

Ideal head rise:

$$\Delta H_i = \frac{U_2 V_{\theta,2}}{g} - \frac{U_1 V_{\theta,1}}{g} = \frac{U_2}{g}\left[U_2 - V_{z,2}\tan(\kappa_2 + \delta)\right] - \frac{U_1 V_{\theta,1}}{g} \tag{B1}$$

Rotor relative total head-loss coefficient:

$$\overline{\omega} = \frac{H'_{2,i} - H'_2}{V_1'^2/2g} = \frac{\Delta H_i - \Delta H}{V_1'^2/2g} \tag{B2}$$

Blade diffusion factor:

$$D = 1 - \frac{V'_2}{V'_1} + \frac{r_2 V_{\theta,2} - r_1 V_{\theta,1}}{\sigma V'_1(r_1 + r_2)} \tag{B3}$$

or, for $r_1 = r_2$

$$D = 1 - \frac{V'_2}{V'_1} + \frac{\Delta V_\theta}{2\sigma V'_1} $$

Efficiency:

$$\eta = \frac{\Delta H}{(\Delta H)_i} \tag{B4}$$

Cavitation number:

$$k = \frac{h_1 - h_v}{V_1'^2/2g} \tag{B5}$$

Head-rise coefficient:

$$\psi = \frac{g\,\Delta H}{U_t^2} \tag{B6}$$

31

Ideal head-rise coefficient:

$$\psi_i = \frac{g \ \Delta H}{U_t^2}$$

Flow coefficient:

$$\varphi = \frac{V_z}{U_t} \tag{B7}$$

Incidence angle:

$$i = \beta_1' - \kappa_1 \tag{B8}$$

Deviation angle:

$$\delta = \beta_2' - \kappa_2 \tag{B9}$$

Overall and Averaged Parameter Equations

Mass-averaged total head:

$$\overline{\Delta H} = \frac{\displaystyle\int_{r_h}^{r_t} \Delta H \ V_z r \ dr}{\displaystyle\int_{r_h}^{r_t} V_z r \ dr} \tag{B10}$$

Mass-averaged efficiency:

$$\overline{\eta} = \frac{\displaystyle\int_{r_h}^{r_t} \eta V_z r \ dr}{\displaystyle\int_{r_h}^{r_t} V_z r \ dr} \tag{B11}$$

Mass-averaged head-rise coefficient:

$$\overline{\psi} = \frac{\overline{H}_2 - \overline{H}_1}{U_t^2 / g} \tag{B12}$$

32

Average inlet axial velocity:

$$\overline{V}_{z,1} = \frac{144Q_m}{448.8 \; \pi\left(r_{t,1}^2 - r_{h,1}^2\right)} \tag{B13}$$

Average inlet-flow coefficient:

$$\overline{\varphi}_1 = \frac{\overline{V}_{z,1}}{U_t} \tag{B14}$$

Average blade cavitation number:

$$\overline{k} = \frac{2gH_{sv}}{U^2\left(1 + \overline{\varphi}_1^2\right)} - \frac{\overline{\varphi}_1^2}{1 + \overline{\varphi}_1^2} \tag{B15}$$

Net positive suction head:

$$H_{sv} = H_1 - h_v \tag{B16}$$

REFERENCES

1. Members of the Compressor and Turbine Research Division: Aerodynamic Design of Axial-Flow Compressors, vol. II. NACA RM E56B03a, 1956.

2. Crouse, James E., Montgomery, John C., and Soltis, Richard F.: Investigation of the Performance of an Axial-Flow-Pump Stage Designed by the Blade-Element-Theory - Design and Overall Performance. NASA TN D-591, 1961.

3. Crouse, James E., Soltis, Richard F., and Montgomery, John C.: Investigation of the Performance of an Axial-Flow-Pump Stage Designed by the Blade-Element Theory - Blade-Element Data. NASA TN D-1109, 1961.

4. Crouse, James E., and Sandercock, Donald M.: Design and Overall Performance of an Axial-Flow-Pump Rotor with a Blade Tip Diffusion Factor of 0.43. NASA TN D-2295, 1964.

5. Lieblein, Seymour, Schwenk, Francis C., and Broderick, Robert L.: Diffusion Factor for Estimating Losses and Limiting Blade Loadings in Axial-Flow-Compressor Blade Elements. NACA RM E53D01, 1953.

6. Herrig, L. Joseph, Emery, James C., and Erwin, John R.: Systematic Two-Dimensional Cascade Tests of NACA 65-Series Compressor Blades at Low Speeds. NASA TN 3916, 1957.

7. Lieblein, Seymour, and Roudebush, William H.: Theoretical Loss Relations for Low Speed Two-Dimensional-Cascade Flow. NACA TN-3662, 1956.

8. Lieblein, Seymour: Analysis of Experimental Low-Speed Loss and Stall Characteristics of Two-Dimensional Compressor Blade Cascades. NACA RM E57A28, 1957.

9. Lysen, J. C., and Serovy, G. K.: Estimation of the Velocity Distribution at the Inlet of an Axial-Flow Turbomachine. Paper 63-WA 162, ASME, 1963.

NASA SCIENTIFIC AND TECHNICAL PUBLICATIONS

TECHNICAL REPORTS: Scientific and technical information considered important, complete, and a lasting contribution to existing knowledge.

TECHNICAL NOTES: Information less broad in scope but nevertheless of importance as a contribution to existing knowledge.

TECHNICAL MEMORANDUMS: Information receiving limited distribution because of preliminary data, security classification, or other reasons.

CONTRACTOR REPORTS: Technical information generated in connection with a NASA contract or grant and released under NASA auspices.

TECHNICAL TRANSLATIONS: Information published in a foreign language considered to merit NASA distribution in English.

TECHNICAL REPRINTS: Information derived from NASA activities and initially published in the form of journal articles.

SPECIAL PUBLICATIONS: Information derived from or of value to NASA activities but not necessarily reporting the results of individual NASA-programmed scientific efforts. Publications include conference proceedings, monographs, data compilations, handbooks, sourcebooks, and special bibliographies.

Details on the availability of these publications may be obtained from:

SCIENTIFIC AND TECHNICAL INFORMATION DIVISION

NATIONAL AERONAUTICS AND SPACE ADMINISTRATION

Washington, D.C. 20546